In Situ Electron Energy Loss Spectroscopy Studies of Gas-Dependent Metal−Support Interactions in Cu/ZnO Catalysts

Jakob B. Wagner,[†,‡] Poul L. Hansen,[†] Alfons M. Molenbroek,[†] Henrik Topsøe,[†] Bjerne S. Clausen,[†] and Stig Helveg*[,†]

Haldor Topsøe A/S, Nymøllevej 55, DK-2800 Kgs. Lyngby, Denmark, and NBIfAFG, University of Copenhagen, Universitetsparken 5, DK-2100 Copenhagen Ø, Denmark

Received: December 20, 2002; In Final Form: April 8, 2003

The metal−support interaction in a Cu/ZnO catalyst is investigated using in situ electron energy loss spectroscopy (EELS) with a resolution better than 1.3 eV. We focus on the energy loss near edge structure (ELNES) at the Cu L_3 ionization edge. The intensity of the ELNES changes, reflecting modifications in the electronic structure of Cu, for the catalyst treated in gas environments of different reduction potential. The ELNES intensity data are compared with results for bulk reference spectra and spectra calculated using FEFF8.0. On this basis, the changes in the ELNES are interpreted as a tensile strain in the Cu nanoclusters induced by the ZnO support and a Cu−Zn alloy formation induced to a degree depending on the severity of the reduction treatment of the catalyst. For Cu/SiO_2 catalysts, both the support and the reduction potential of the gas have only negligible influence on the structure and the ELNES of the Cu nanocrystals.

1. Introduction

The nature of the support has important influence on the properties of supported metal catalysts.[1−3] In general, the interaction between the metal and the support plays a key role in the determination of the size and the shape of the metal nanoclusters and, hence, the distribution of active sites. Furthermore, the metal−support interaction may cause electronic or compositional modifications of the exposed metal facets. One attractive possibility for obtaining fundamental insight is to employ well-defined model systems and to elucidate metal−support interactions under idealized vacuum conditions.[4−7] However, the metal, support, and interface free energies may change depending on the gas conditions encountered during catalysis, and structural transformations may therefore occur with dramatic consequences for the catalyst properties.[8] This emphasizes the need for characterizing the metal−support interactions of catalysts in situ under relevant gas conditions.[9]

The important Cu/ZnO-based methanol synthesis catalysts have been studied extensively, e.g., see ref 10. Although metal-like copper particles are believed to be the active species, several different types of interactions with ZnO have also been discussed to be of importance. It has for example been considered that shape changes of the Cu particles occur depending on the composition of the gas phase,[8,11] that the ZnO induces a strain in the Cu particles,[12] and that a Cu−Zn alloy forms under severe reduction conditions.[8,13−15] Recently, we have studied directly the way in which the shape and the structure of Cu nanocrystals supported on ZnO change according to variations in the gas atmosphere using in situ high-resolution transmission electron microscopy (TEM).[16] In particular, we found in accordance with previous work[8,11] that the Cu nanoclusters have an increased tendency to wet the ZnO support as the reduction potential of the gas phase increases. A quantitative analysis of the TEM images showed that the interface energy decreased correspondingly by 1.2 J/m^2. On the basis of the TEM results alone, the driving force underlying the structural transformations could not be inferred.

In the present paper, we derive insight into the Cu−ZnO interaction under different gas conditions by combining the in situ TEM results with in situ electron energy loss spectroscopy (EELS) measurements. We focus on the energy loss near edge fine structure (ELNES) of the Cu L_3 ionization edge. Because the ELNES reflects the local electronic structure of the excited Cu atoms, it provides an indirect structure-sensitive measure.[17,18] By comparing the ELNES data with results from bulk reference spectra and simulated spectra, variations in the ELNES are attributed to a tensile strain in the Cu nanocrystals, which is induced by the ZnO support, and a Cu−Zn alloy formation, which is associated with a gas-induced decrease in Cu−ZnO interface energy.

2. Experimental Details

2.1. Sample Preparation. The Cu/ZnO model catalyst is prepared using flame synthesized ZnO crystallites (∼100 nm wide).[19] The ZnO support is impregnated with an aqueous solution of Cu−acetate. After impregnation and drying, the sample is heated in a flow of 2% O_2 in Ar at 400 °C for 4 h. Specimens are obtained by dispersing powders of the calcined catalyst in dry form onto a molybdenum TEM grid.

The SiO_2 support consists of ∼600 nm wide spherical particles which are synthesized according to ref 20. The Cu/SiO_2 catalyst is prepared in the same way as the Cu/ZnO catalyst.

Bulk copper references are prepared from a Cu foil with a nominal purity of 99.99% and electro-polished to produce a thin, circular, wedge-shaped region centered on the sample. Bulk brass references are prepared in the same way from a $Cu_{67}Zn_{33}$ foil.

2.2. EELS Measurements. The experiments are carried out in a Philips CM300 field emission gun (FEG) instrument,

* To whom correspondence should be addressed. E-mail: sth@topsoe.dk.
† Haldor Topsøe A/S.
‡ University of Copenhagen.

10.1021/jp0277863 CCC: $25.00
Published on Web 07/02/2003

equipped with a differential pumped in situ cell as described in ref 21. In the in situ cell, samples can be exposed to gas pressures up to 20 mbar and heated to about 900 °C, depending on the gas pressure and composition. Under these in situ conditions, high-resolution TEM images can be obtained with a resolution better than 1.4 Å. Furthermore, high-resolution EELS spectra can be acquired using a Gatan Image Filter (GIF-2000) controlled by the Gatan Digital Micrograph software. The resolution of the EEL spectra is defined as the full width at half-maximum of the zero-loss peak and is less than 1.3 eV.

In the HRTEM mode, the electron beam has a convergence angle less than 0.2 mrad. The EEL spectra are recorded in the diffraction mode with a camera length of 335 mm and a 3.0 mm entrance aperture to the spectrometer, corresponding to a collection semiangle of 4.5 mrad. These angles minimize the contribution from multipole excitations.[18]

Spectra at the Cu $L_{2,3}$ edges are recorded with a dispersion of 0.1 eV in an energy window of about 100 eV. Each spectrum consists of 20−30 single spectra acquired cumulatively, each with an exposure time of 20 s. The EEL spectra are acquired from areas containing about 10 Cu nanoclusters, and for each sample, spectra are recorded from at least five different areas. The energy loss spectra are acquired from areas less than 20 nm in thickness in order to minimize multiple scattering effects. The thickness of the areas is estimated using the log-ratio method.[18]

The raw spectra are processed by background subtraction, and plural scattering is removed using the Fourier-ratio deconvolution in the Gatan EL/P software. The Cu L_3 edge onset is set to 930 eV in the processed spectra. An absolute energy calibration was not possible because the samples do not contain an internal reference in the resolved energy window. The spectra are normalized to be independent of the electron beam intensity and the amount of specimen by scaling the intensity so that the distinct minimum at 947 eV becomes unity in all spectra.[22] The position of the minimum is determined by fitting a fourth order polynomial to each spectrum in the energy interval 942−952 eV.

In the normalized spectra, the intensity at the Cu L_3 edge is integrated over 17 eV from $E(L_3) = 930$ eV. From the area below unity intensity, the contribution to the integral is constant in all spectra and reflects largely the basic ionization edge shape. From the area above unity intensity (the hatched areas in Figure 1), the contribution to the integral is referred to as the ELNES intensity. The fine structure of the Cu L_3 edge largely reflects the density of states (DOS) above the Fermi level.[23] Variations in the ELNES intensity therefore provide a simple measure of changes in the integrated DOS.

2.3. FEFF Calculations. Spectra at the Cu L_3 edge are simulated within the multiple scattering approach using the FEFF8.0 software package.[24] The ELNES calculations are based on the dipole approximation for electronic excitation which is valid for scattering angles less than 10 mrad.[18] In the ELNES calculations, self-consistent scattering potentials are used. The iterative calculations of the potentials converged within 10 cycles. Thermal disorder is included using the Debye model with a Debye temperature of 42 °C and a simulation temperature of 25 °C. We find no significant deviation in a spectrum calculated at 220 °C, at which the EEL spectra are acquired.

Spectra of the Cu L_3 edge are calculated with a bulk model for copper using (a) the initial state approach (no core hole) and (b) the final state approach (full core hole). To account for the fact that the ionization is a dynamic process, a noninteger electron occupation number must be assigned to the initial core state.[25] Here the effect of a partial core hole is described by linearly combining spectra calculated using (a) and (b). To a first approximation, we expect this combination to be independent of the surroundings of the excited Cu atom and calibrate the weighting factors by fitting the linear combination for bulk Cu to the experimental data (Figure 1, VI). We obtain the weights 0.8 and 0.2 for (a) and (b), respectively. All other simulated spectra are obtained using this linear combination of (a) and (b). The simulated spectra are normalized by scaling the intensity so the minimum at 947 eV becomes unity.

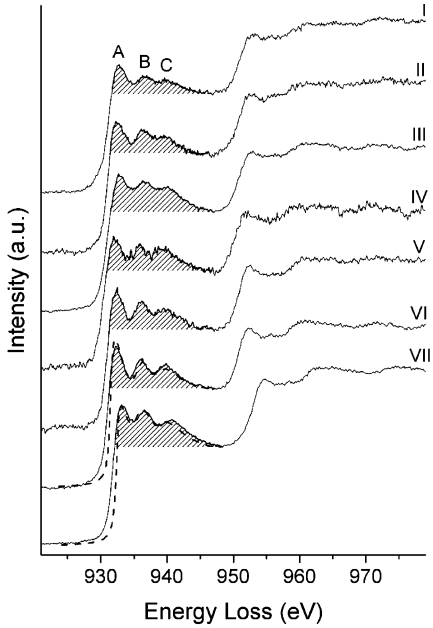

Figure 1. In situ EEL spectra at the Cu $L_{2,3}$ edges. The spectra are acquired from (I) Cu/ZnO (in 1.5 mbar H_2 at 220 °C), (II) Cu/ZnO (in a H_2(85%) and CO(15%) mixture at a total pressure of 1.5 mbar at 220 °C, after heating to 280 °C for 1 h), (III) Cu/ZnO (in a H_2(85%) and CO(15%) mixture at a total pressure of 1.5 mbar at 220 °C, after heating to 450 °C for 1 h), (IV) Cu/SiO_2 (in 1.5 mbar H_2 at 220 °C), (V) Cu/SiO_2 (in a H_2(85%) and CO(15%) mixture at a total pressure of 1.5 mbar at 220 °C, after heating to 280 °C for 1 h), (VI) the Cu foil (in 1.5 mbar H_2 at 220 °C), and (VII) the brass foil (in 1.5 mbar H_2 at 220 °C). The spectra are all normalized according to the procedure described in the text. The ELNES intensities are obtained by integration of the hatched areas. The dashed lines in VI and VII correspond to simulated spectra.

3. Results

3.1. EELS Measurements. For the calcined Cu/ZnO catalyst, the ELNES at the Cu $L_{2,3}$ edges shows two adsorption jumps at $E(L_3) = 930$ eV and $E(L_2) = 950$ eV. The white-lines at the apex of the edges are attributed to transitions from 2p core levels to unoccupied 3d levels present in oxidized copper.[17] Furthermore, from a comparison with spectra of CuO and Cu_2O powder references, it is concluded that copper in the as-prepared catalyst is primarily in the Cu(II) oxidation state.

To transform the CuO precursor into Cu nanoclusters, the calcined model catalyst is reduced in 1.5 mbar H_2 at 280 °C for 1 h. Subsequently, the temperature is decreased to 220 °C. This reduction procedure results in 3−6 nm wide Cu clusters having a stable and facetted morphology (Figure 2). From in situ high-resolution TEM images (Figure 2b), lattice fringes are seen in the Cu nanocrystals with separations of 0.21 nm and 0.18 nm. These are assigned to the (111) and (200) lattice planes in metallic copper, respectively. Thus, the reduction procedure

TABLE 1: Relative Positions ($|i-j|$) and Heights (h_i) of the Spectral Features (i,j = A, B, and C) and the ELNES Intensity Obtained from the Normalized EEL Spectra at the Cu L_3 Ionization Edge

		|A−B| (eV)	|A−C| (eV)	h_A	h_B	h_C	ELNES intensity
experimental	I	3.87(0.20)	7.37(0.50)	1.29(0.02)	1.18(0.02)	1.14(0.02)	1.70(0.21)
spectra	II	3.83(0.20)	7.38(0.50)	1.35(0.04)	1.27(0.03)	1.21(0.03)	2.26(0.25)
	III	3.78(0.20)	7.60(0.50)	1.39(0.04)	1.29(0.02)	1.22(0.04)	2.63(0.29)
	IV	3.83(0.20)	7.27(0.50)	1.36(0.06)	1.30(0.02)	1.23(0.03)	2.33(0.25)
	V	3.77(0.20)	7.70(0.50)	1.39(0.03)	1.28(0.02)	1.21(0.01)	2.29(0.21)
	VI	3.80(0.20)	7.65(0.50)	1.42(0.02)	1.31(0.02)	1.25(0.02)	2.47(0.30)
	VII	2.87(0.20)	6.77(0.50)	1.43(0.02)	1.40(0.04)	1.28(0.03)	3.28(0.33)
simulated spectra	0%Zn, a = 0.95*a_{Cu}	4.70(0.20)	8.30(0.40)	1.51(0.02)	1.27(0.02)	1.21(0.02)	2.62
	0%Zn, a = a_{Cu}	4.10(0.20)	7.50(0.40)	1.49(0.02)	1.26(0.02)	1.20(0.02)	2.29
	0%Zn, a = 1.05*a_{Cu}	3.60(0.20)	6.80(0.40)	1.46(0.02)	1.24(0.02)	1.18(0.02)	1.96
	0% Zn, a = a_{Cu}	4.10(0.20)	7.50(0.40)	1.49(0.02)	1.26(0.02)	1.20(0.02)	2.29
	10% Zn, a = a_{Cu}	3.80(0.20)	7.30(0.40)	1.50(0.02)	1.31(0.02)	1.21(0.02)	2.54
	20% Zn, a = a_{Cu}	3.00(0.20)	6.30(0.40)	1.41(0.02)	1.39(0.02)	1.25(0.02)	2.70
	33% Zn, a = a_{Cu}	2.80(0.20)	6.10(0.40)	1.39(0.02)	1.40(0.02)	1.26(0.02)	2.78
	50% Zn, a = a_{Cu}	2.50(0.20)	5.90(0.40)	1.39(0.02)	1.42(0.02)	1.25(0.02)	2.83
	33% Zn, a = 1.05*a_{Cu}	2.40(0.20)	5.40(0.40)	1.40(0.02)	1.39(0.02)	1.24(0.02)	2.52

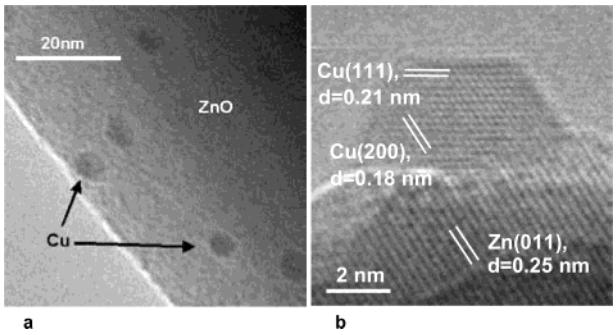

Figure 2. In situ TEM images of the Cu/ZnO catalyst. The images are acquired with the sample in 1.5 mbar H_2 and at T = 220 °C. (a) The low-magnified image shows an ensemble of 3−6 nm wide Cu nanoclusters. (b) High-magnified image of a Cu nanocrystal. The lattice fringes in the copper nanocrystal correspond to the (111) and (200) planes of metallic copper.

results in metallic Cu nanocrystals. For the calcined Cu/SiO_2 catalyst, the reduction in H_2 also results in 3−6 nm wide Cu nanocrystals.

EEL spectra are acquired in situ at the Cu $L_{2,3}$ edges of the metallic Cu nanocrystals (Figure 1, I): The characteristic CuO white-lines have disappeared. At the Cu L_3 edge, three maxima have emerged and will be referred to as A, B, and C. At the Cu L_2 edge, less distinct features are formed.

It should be stressed that the ability to perform in situ studies is of utmost importance for studying Cu-based catalysts in their catalytic active metallic state. If the reduced catalyst is exposed to air at room temperature, the Cu nanoclusters reoxidize as revealed from the ELNES displaying the oxidic white-lines. Furthermore, the reoxidation happens even if the reduced catalyst sample is left at room temperature in the TEM column having a base pressure of 1×10^{-7} Torr.

Changes in the gas composition can induce marked changes in the shape of the Cu nanocrystals.[16] Here we investigate the effect of increasing the reduction potential of the gas phase by adding carbon monoxide to the H_2 gas. The Cu/ZnO system is heated to 280 °C or 450 °C for 1 h in a gas mixture of $CO:H_2$ = 0.15:0.85 at 1.5 mbar. This procedure transforms the Cu nanocrystals into disklike structures as revealed by in situ TEM imaging.[16] In situ EEL spectra are acquired of the Cu/ZnO sample after the H_2/CO treatments (Figure 1, II and III). In the spectra I−III, the relative heights and positions of the spectral features A, B, and C are seen to be constant within the experimental scatter (Table 1), whereas the amplitude of the normalized spectra is seen to increase in the near-edge region as the reduction conditions become more severe (Figure 3).

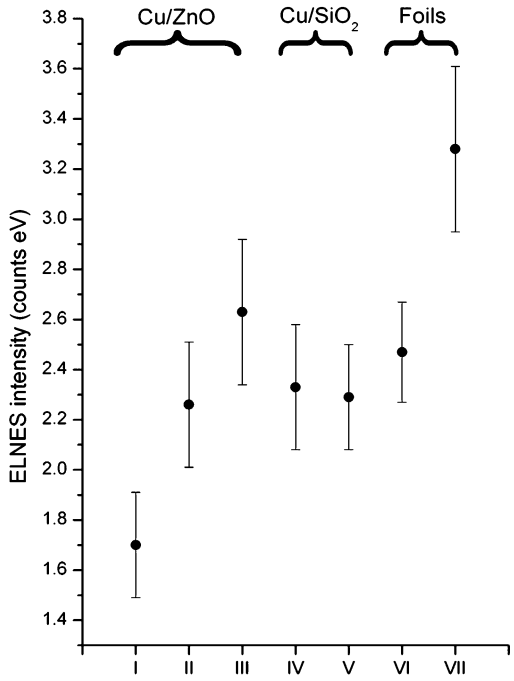

Figure 3. ELNES intensity of the normalized experimental spectra from the Cu L_3 ionization edge. For each sample, the mean value and the standard deviation are obtained from 5 spectra from different areas.

The gas-induced morphological changes appear to depend on the nature of the support. In fact, the spectra of the Cu/SiO_2 catalyst are independent of the reduction potential of the gas and they are similar to that of the Cu foil (Figure 1). Furthermore, the Cu nanocrystals on SiO_2 do not tend to wet the support as the reduction potential of the gas phase is increased.[11,16] This suggests a key role of the ZnO support in the structural transformations described above. Spectra IV and V are acquired of Cu nanocrystals on SiO_2 in situ under conditions similar to those applied to the Cu/ZnO catalyst in spectra I and II. In spectra IV and V, the relative heights and positions of the spectral features A, B, and C, as well as the ELNES intensity, remain constant reflecting the stable shape of the Cu nanocrystals on SiO_2 (Table 1 and Figure 3).

It has been proposed that reduction at high temperature facilitates a Cu−Zn surface or bulk alloy formation in ZnO-supported Cu nanoclusters.[8,13] Hence, for comparison, we have acquired EEL spectra of a Cu (Figure 1, VI) and a $Cu_{67}Zn_{33}$ (Figure 1, VII) foil. For the as-prepared foils, we find white-lines in the EEL spectra corresponding to Cu oxide. The foils

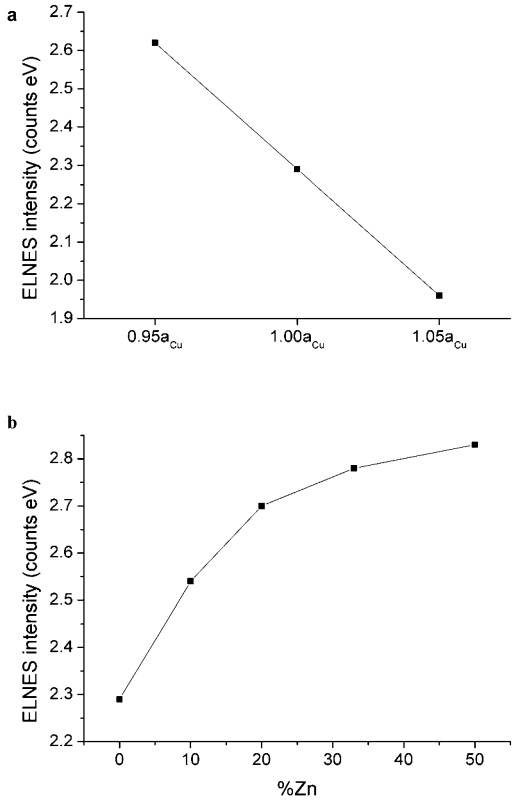

Figure 4. ELNES intensity of simulated spectra of the Cu L_3 ionization edge. The simulations address the influence of (a) strain in Cu lattice and (b) Zn alloyed into the Cu.

are therefore reduced in the TEM in 1.5 mbar H_2 at 220 °C for 1 h, before in situ acquisition of EEL spectra. The relative heights and positions of the features A, B, and C in spectra VI and VII are found to change slightly (Table 1). Furthermore, the ELNES intensity is larger for VII than for VI (Figure 3).

3.2. FEFF Calculations. Spectra are simulated at the Cu L_3 edge in order to shed light on the structural transformations causing variations in the ELNES intensity. A calculated spectrum for bulk Cu (lattice constant of $a_{Cu} = 0.361$ nm) is included in Figure 1 for comparison with the experimental spectrum VI, and a calculated spectrum for a bulk $Cu_{67}Zn_{33}$ alloy (with an fcc lattice constant $a_{brass} = 0.370$ nm) is compared with the spectrum VII. Furthermore, the position and the peak height of A, B, and C, as well as the ELNES intensity of the calculated spectra, are included in Table 1. It is seen that the calculated spectra compare well with the experimental spectra demonstrating that the FEFF calculations can reproduce the features and trends of the ELNES at the Cu L_3 edge. The calculated peak positions, heights, and ELNES intensities differ, however, from the experimentally observed values by 10−20% (see Table 1), and we have therefore chosen only to use the calculated spectra for a qualitative comparison with the measured spectra.

The influence of strain in the Cu L_3 EELS spectra has been evaluated. Spectra are calculated for a Cu lattice with the bulk lattice constant, with 5% tensile strain and with 5% compressive strain. For the spectral features A, B, and C, the relative peak positions shift to lower energy loss and the intensities are observed to decrease as the lattice constant increases (Table 1). Figure 4a shows that the ELNES intensity decreases with an increasing lattice parameter.

To address the issue of Cu−Zn alloy formation, spectra of bulk Cu−Zn alloys are simulated for different Cu/Zn atomic ratios. Cu_xZn_{1-x} alloy structures are prepared by randomly substituting Zn atoms into Cu fcc positions. The lattice constant is set to a_{Cu}. Changes in the fine structure of the Cu L_3 edge are observed. For the spectral features A, B, and C, the relative peak positions shift toward lower energy loss and the intensities increase for an increasing amount of Zn in the Cu lattice (Table 1). Figure 4b shows that the ELNES intensity of the Cu L_3 edge increases for larger amounts of substituted Zn atoms.

In bulk brass ($Cu_{67}Zn_{33}$), the lattice is expanded and Zn is substituted into fcc sites as compared with bulk Cu, suggesting a competition between the effect of tensile strain and alloying on the Cu L_3 ELNES. To evaluate their relative strength, we have calculated a spectrum for a $Cu_{67}Zn_{33}$ alloy with a lattice constant $a = 1.05a_{Cu}$. The spectral features listed in Table 1 clearly show that the effect of the Cu−Zn alloy dominates the effect of strain.

In the calculations, we use a bulk model for copper (and brass). However, the Cu clusters in the model catalysts (Cu/ZnO and Cu/SiO_2) are 3−6 nm wide, corresponding to a dispersion of 0.33−0.17 (calculated as the ratio of the number of surface atoms to total number of atoms in the cluster, which is assumed to have a half-spherical shape). We have addressed the influence of the finite particle size on the EEL spectra by calculating spectra for Cu clusters containing up to 249 Cu atoms (corresponding to a cluster diameter of 1.8 nm). The cluster spectra are calculated by averaging spectra obtained from all of the Cu atoms in the cluster. It is found that the spectral feature A at 933 eV achieves an intensity close to that for bulk Cu for clusters with more than 79 atoms (cluster diameter = 1.1 nm). The spectral features B and C appear for clusters containing more than 135 atoms (cluster diameter = 1.4 nm). Thus, we find that the cluster spectra rapidly approach the bulk Cu spectra with increasing size of the Cu cluster. In fact, the ELNES features are found to be dominated by multiple scattering out to the third coordination shell from the excited atom. We therefore expect that reduced coordination or other effects on the surface atoms will have only limited influence on the spectra.

4. Discussion

The results presented here emphasize the importance of studying Cu-based catalysts in situ under controlled gas conditions. Furthermore, the results show that in situ ELNES studies may give important insight into gas-induced changes in the detailed structure of the supported Cu nanocrystals. Below we will discuss the observed variations in the ELNES intensity for the Cu nanocrystals treated in gases of varying reduction potential in the light of the FEFF calculations.

For copper reduced in hydrogen, the ELNES intensity for Cu/ZnO (I) is smaller than that for Cu/SiO_2 (IV), which is similar to that for the Cu foil (VI). Because the Cu nanocrystals have similar size and shape in the two catalysts and because the cluster size is in a range where the surface atoms have a minor influence on a spectrum, the difference in the ELNES intensity between spectra I and VI may reflect modifications of the Cu lattice in the Cu/ZnO system. One possible explanation is that the Cu nanocrystals are strained due to epitaxial mismatch with the ZnO support. The FEFF calculations show that a tensile strain of the Cu lattice causes a downshift in the ELNES intensity. We therefore attribute the difference in ELNES intensity to an epitaxial strain in Cu nanocrystals supported on ZnO. For Cu on SiO_2, the lattice is essentially unperturbed relative to bulk Cu.

A tensile strain in the Cu nanocrystals may be expected to be resolved in high-resolution TEM images.[26] We therefore

examined images (such as Figure 2b) in detail and found only interatomic distances corresponding to those for bulk copper within 5%. To address the limit beyond which strain is distinguishable in the experimental high-resolution images at all, image simulations of Cu nanocrystals on ZnO were performed using the EMS[27] and the Rhodius[28] software packages. We find that electron-optical effects, tilt of the particle with respect to the electron beam, and varying thickness along the projected particle shape may disguise up to 5% strain in the Cu nanocrystals.[23] Furthermore, the Cu planes closest to the ZnO are expected to be the most strained layers. These planes may not be observed in the images due to the roughness of the ZnO support or due to the fact that the Cu/ZnO interface may not be exactly parallel to the electron beam.

Addition of CO to the hydrogen gas increases the reduction potential of the gas environment for the Cu/ZnO system. The Cu nanocrystals are observed to respond to this by an increased wetting of the ZnO support,[16] and consequently, an even more pronounced effect of epitaxial strain could be expected. At first sight, this is in variance with the increasing ELNES intensities in spectra I−III. Thus, the results indicate that another type of metal−support interaction is dominating the observed intensities under the more severe reduction conditions. Because a similar increase of the ELNES intensity is also observed going from the Cu metal to the Cu−Zn alloy foil (spectra VI and VII), we suggest that a Cu−Zn alloy formation is induced in the Cu/ZnO catalyst under the more reducing conditions. This is also corroborated by the FEFF calculations showing that a substitution of Zn into the Cu lattice causes an increasing ELNES intensity. It has been suggested that the larger reduction potential of the H_2/CO mixture as compared with H_2 will increase the amount of O vacancies in the surface of the ZnO support.[8,11] This decreases the Cu/ZnO_x interface energy and increases the tendency for alloy formation due to the miscibility of Cu and Zn. Thus, the present results indicate that the morphological change of the Cu nanocrystals is accompanied by an increased tendency for a Cu−Zn alloy formation at high temperature in the more reducing gas. It should be noted that a pure Cu lattice and a Cu−Zn alloy cannot be distinguished in high-resolution TEM images because Cu and Zn have almost the same scattering power. Furthermore, the ELNES intensity of spectrum III is lower than that of VII. We expect this to be due to the part of the Cu/ZnO interface originating from the H_2 reduction of the as-prepared catalyst. This part of the interface, which is still present under the more reducing conditions in spectra II and III, will shift down the ELNES intensity and hence counteract the effect of Cu−Zn alloy formation. However, the difference between spectrum III and spectrum VII could also reflect a Zn content being lower than that for the reference foil, according to Figure 4.

For the Cu/SiO_2 system, the ELNES intensities in IV and V are constant reflecting that no structural changes of the Cu nanocrystals are observed. This is expected because the formation of oxygen vacancies in the surface of SiO_2 is more difficult than in ZnO due the relative higher Si−O bond strength.[11] Hence, the reduction potential in the gas phase should have less influence on the interface energy than for the Cu/ZnO system.

In the models used in the FEFF calculations, the strain of the Cu lattice is distributed isotropic and the Cu−Zn alloys are homogeneous (random). This is most likely not the case in the Cu/ZnO catalysts, where a tensile strain and a Zn content in the Cu lattice are expected to be larger near the Cu/ZnO interface. Structural anisotropy and inhomogeneity will broaden the spectral features A, B, and C, and because the ELNES intensity in the spectra of the nanoclusters is also relatively small, small shifts in the spectral features will be difficult to detect. This is probably the reason that no significant shift is observed of the relative peak positions and heights for the spectral features A, B, and C in the catalysts, whereas shifts are seen for the reference foils and in the FEFF calculations.

A summary of the results indicate that the metal−support interaction in the Cu/ZnO system depends on the gas environment and originates from a combined effect of epitaxial strain, shape dynamics, and alloy formation. The special synergy in the Cu/ZnO catalyst systems may be related to such interactions. A more systematic study of each of these effects under reaction conditions is required in order to evaluate which one plays the dominating role for the catalyst activity.

5. Conclusions

By combining in situ high-resolution TEM and EELS, the metal−support interaction is investigated in the Cu/ZnO system. Variations in the ELNES intensity at the Cu L_3 edge are interpreted as a tensile strain in the Cu nanoclusters induced by the ZnO support and a Cu−Zn alloy formation at the Cu/ZnO interface induced by increasing the reduction potential in the gas phase. The alloy formation is associated with a conformational transformation of the facetted Cu nanoclusters into disklike structures.

The combined in situ EELS/TEM approach presented here should be applicable in general to investigate complex gas-dependent metal−support interactions involving both morphological and electronic interactions in supported nanocluster systems.

Acknowledgment. We thank E. Johnson for fruitful discussions and T. Johannesen and H. Teunissen for preparation of the catalysts. J.B.W. acknowledges the Danish Research Academy for supporting a scholarship at the Interdisciplinary Center of Catalysis (ICAT). S.H. acknowledges support from the Danish Research Council STVF. The CTCI foundation in Taipei, Taiwan is gratefully acknowledged for financial contribution to the in situ TEM facility.

References and Notes

(1) Baker, R. T. K., Tauster, S. J., Dumesic, J. A., Eds.; *Strong Metal-Support Interactions*; American Chemical Society: Washington, DC, 1986.
(2) Hammer, B.; Nørskov, J. K. *Adv. Catal.* **2000**, *45*, 71.
(3) Datye, D. *J. Catal.* **1995**, *155*, 148.
(4) Champbell, C. *Surf. Sci. Rep.* **1997**, *27*, 1.
(5) Bäumer, M.; Freund, H.-J. *Prog. Surf. Sci.* **1999**, *61*, 127.
(6) Henry, C. R. *Surf. Sci. Rep.* **1998**, *31*, 231.
(7) Hansen, K. H.; Worren, T.; Stempel, S.; Bäumer, M.; Freund, H.-J.; Besenbacher, F.; Stensgaard, I. *Phys. Rev. Lett.* **1999**, *83*, 4120.
(8) Grunwaldt, J.-D.; Molenbroek, A. M.; Topsøe, N.-Y.; Topsøe, H.; Clausen, B. S. *J. Catal.* **2000**, *194*, 452.
(9) Topsøe, H. *J. Catal.* **2003**, *216*, 155.
(10) Hansen, J. B. In *Handbook of Heterogeneous Catalysis*; Ertl, G., Knözinger, H., Weitkamp, J., Eds.; VHC: Weinheim, 1997; Vol. 4.
(11) Clausen, B. S.; Schiøtz, J.; Gråbæk, L.; Ovesen, C. V.; Jacobsen, K. W.; Nørskov, J. K.; Topsøe, H. *Top. Catal.* **1994**, *1*, 367.
(12) Günther, M. M.; Ressler, T.; Bems, B.; Büscher, C.; Genger, T.; Hindrichsen, O.; Muhler, M.; Schlögl, R. *Catal. Lett.* **2001**, *71*, 37.
(13) Topsøe, N.-Y.; Topsøe, H. *Top. Catal.* **1999**, *8*, 267.
(14) Fujitani, T.; Nakamura, J. *Catal. Lett.* **1998**, *56*, 119.
(15) Greeley, J.; Gokhale, A. A.; Kreuser, J.; Dumesic, J. A.; Topsøe, H.; Topsøe, N.-Y.; Mavrikakis, M. *J. Catal.* **2002**, *213*, 63.
(16) Hansen, P. L.; Wagner, J. B.; Helveg, S.; Rostrup-Nielsen, J. R.; Clausen, B. S.; Topsøe, H. *Science* **2002**, *295*, 2053.
(17) Keast, V. J.; Scott, A. J.; Brydson, R.; Williams, D. B.; Bruley, J. *J. Microsc.* **2001**, *203*, 135.
(18) Egerton, R. F. *Electron Energy-Loss Spectroscopy in the Electron Microscope*; Plenum Press: New York, 1996.

(19) Reimer, J. R.; Johannesen, T.; Wedel, S.; Livbjerg, H. *J. Nanoparticle Res.* **2000**, *2*, 363.

(20) Stober, W.; Fink, A.; Bohn, E. *J. Colloid Interface Sci.* **1968**, *26*, 82.

(21) Hansen, T. W.; Hansen, P. L.; Wagner, J. B.; Dahl, S.; Topsøe, H.; Jacobsen, C. J. H. *Science* **2001**, *294*, 1508.

(22) Gallezot, P.; Weber, R.; Dalla Bella, R. A.; Boudart, M. *Z. Naturforsch*. **1979**, *34a*, 40.

(23) Wagner, J. B. In situ transmission electron microscopy of catalyst particles, Ph.D. Thesis, Haldor Topsøe A/S and University of Copenhagen, Copenhagen, Denmark, 2002.

(24) Ankudinov, A. L.; Ravel, B.; Rehr, J. J.; Conradson, S. D. *Phys. Rev. B* **1998**, *58*, 7565.

(25) Luitz, J.; Maier, M.; Hébert, C.; Schattschneider, P.; Blaha, P.; Schwarz, K.; Jouffrey, B. *Eur. Phys. J.* **2001**, *B21*, 363.

(26) Crozier, P. A.; Tsen, S.-C.; Liu, J.; López-Cartes, C.; Pérez-Omil, J. A. *J. Electron Microsc.* **1999**, *48*, 1015.

(27) Stadelman, P. *Ultramicroscopy* **1987**, *21*, 131.

(28) Bernal, S.; Botana, F. J.; Calvino, J. J.; López-Cartes, C.; Pérez-Omil, J. A.; Rodríguez-Izquierdo, J. M. *Ultramicroscopy* **1998**, *72*, 135.